

# Chapter Number

## Ferroelectricity in Silver Perovskite Oxides

Desheng Fu<sup>1</sup> and Mitsuru Itoh<sup>2</sup>

<sup>1</sup>Shizuoka University,

<sup>2</sup>Tokyo Institute of Technology

Japan

### 1. Introduction

Many ferroelectric oxides possess the ABO<sub>3</sub> perovskite structure (Mitchell, 2002), in which the A-site cations are typically larger than the B-site cations and similar in size to the oxygen anion. Figure 1 shows a schematic drawing for this structure, where the A cations are surrounded by 12-anions in the cubo-octahedral coordination and the B cations are surrounded by 6-anions in the octahedral coordination. An ideal perovskite exhibits a cubic space group *Pm3m*. This structure is centrosymmetric and cannot allow the occurrence of ferroelectricity that is the presence of a switchable spontaneous electric polarization arising from the off-center atomic displacement in the crystal (Jaffe et al., 1971; Lines & Glass, 1977). The instability of ferroelectricity in the perovskite oxides is generally discussed with the Goldschmidt tolerance factor (*t*) (Goldschmidt, 1926 and Fig. 2),

$$t = (r_A + r_O) / \sqrt{2}(r_B + r_O),$$

where  $r_O$ ,  $r_A$ , and  $r_B$  are the ionic radii of the O, A, and B ions. For a critical value  $t=1$ , the cubic paraelectric phase is stable. This unique case can be found in SrTiO<sub>3</sub>, which has an ideal cubic perovskite structure at room temperature and doesn't show ferroelectricity down to the absolute 0 K (Müller & Burkard, 1979). However, ferroelectricity can be induced by the substitution of O<sup>18</sup> in this quantum paraelectric system at  $T < T_c \sim 23$  K (Itoh et al., 1999). When  $t > 1$ , since the B-site ion is too small for its site, it can shift off-centering, leading to the occurrence of displacive-type ferroelectricity in the crystal. Examples of such materials are BaTiO<sub>3</sub> and KNbO<sub>3</sub> (Shiozaki et al., 2001). On the other hand, for  $t < 1$ , the perovskite oxides are in general not ferroelectrics because of different tilts and rotations of BO<sub>6</sub> octahedra, which preserve the inversion symmetry. But exceptions may be found in the Bi-based materials, in which large A-site displacement is observed. This large A-site displacement is essentially attributed to the strong hybridization of Bi with oxygen (Baettig et al., 2005). Similar cases are observed in Pb-based materials, which commonly have large Pb displacement in the A-site (Egami et al., 1998) and strong covalent nature due to the unique stereochemistry of Pb (Cohen, 1992; Kuroiwa et al., 2001).

Although BaTiO<sub>3</sub>- and PbTiO<sub>3</sub>-based ceramics materials have been widely used in electronic industry (Uchino, 1997; Scott, 2000), there remain some importance issues to be solved. One of such challenges is to seek novel compounds to replace the Pb-based materials, which have a large Pb-content and raises concerns about the environmental pollution (Saito et al., 2004; Rodel et al., 2009).

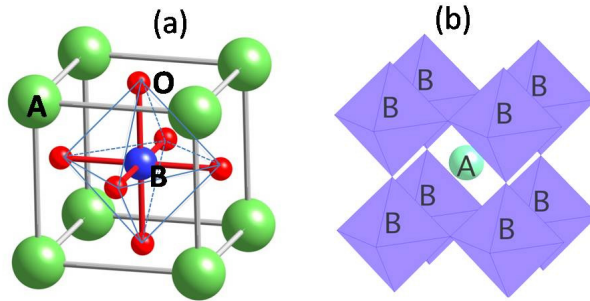


Fig. 1. The structure of an  $ABO_3$  perovskite with the origin centered at (a) the B-site ion and (b) the A-site ion.

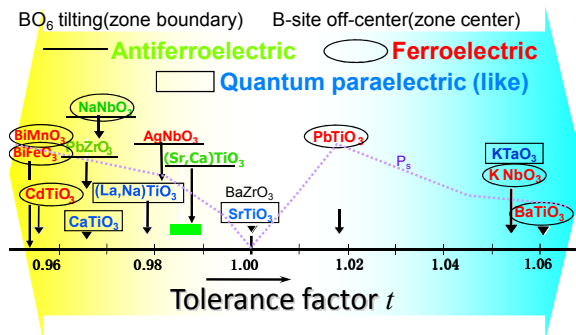


Fig. 2. Tolerance factor of typical dielectric oxides.

The discovery of extremely large polarization ( $52 \mu\text{C}/\text{cm}^2$ ) under high electric field in the  $\text{AgNbO}_3$  ceramics (Fu et al., 2007) indicates that Ag may be a key element in the designs of lead-free ferroelectric perovskite oxides (Fu et al., 2011). With the advance of first-principles calculations (Cohen, 1992) and modern techniques of synchrotron radiation (Kuroiwa et al., 2001), we now know that the chemical bonding in the perovskite oxides is not purely ionic as we have thought, but also possesses covalent character that plays a crucial role in the occurrence of ferroelectricity in the perovskite oxides (Cohen, 1992; Kuroiwa et al., 2001). It is now accepted that it is the strong covalency of Pb with O that allows its large off-center in the A-site. Although Ag doesn't have lone-pair electrons like Pb, theoretical investigations suggest that there is hybridization between Ag and O in  $\text{AgNbO}_3$  (Kato et al., 2002; Grinberg & Rappe, 2003,2004), resulting in a large off-center of Ag in the A-site of perovskite  $\text{AgNbO}_3$  (Grinberg & Rappe, 2003,2004). This prediction is supported by the results from X-ray photoelectron spectroscopy, which suggest some covalent character of the chemical bonds between Ag and O as well as the bonds between Nb and O (Kruczek et al., 2006). Moreover, bond-length analysis also supports such a theoretical prediction. Some of the bond-lengths ( $\sim 2.43 \text{ \AA}$ ) in the structure (Sciau et al., 2004; Yashima et al. 2011) are significantly less than the sum of  $\text{Ag}^+$  ( $1.28 \text{ \AA}$ ) and  $\text{O}^{2-}$  ( $1.40 \text{ \AA}$ ) ionic radii (Shannon, 1967). All these facts make us believe that  $\text{AgNbO}_3$  may be used as a base compound to develop novel ferroelectric materials. Along such a direction, some interesting results have been obtained. It was found

1 that ferroelectricity can be induced through the chemical modification of the  $\text{AgNbO}_3$   
2 structure by substitution of Ag with Li (Fu et al., 2008, 2011), Na (Arioka, 2009; Arioka et al.,  
3 2010), and K (Fu et al., 2009a). Large spontaneous polarization and high temperature of  
4 para-ferroelectric phase transition were observed in these solid solutions. In the following  
5 sections, we review the synthesis, structure, and dielectric, piezoelectric and ferroelectric  
6 properties of these solid solutions together with another silver perovskite  $\text{AgTaO}_3$  (Soon et  
7 al., 2009, 2010), whose solid solutions with  $\text{AgNbO}_3$  are promising for the applications in  
8 microwaves devices due to high dielectric constant and low loss (Volkov et al. 1995; Fortin  
9 et al., 1996; Petzelt et al., 1999; Valant et al., 2007a).

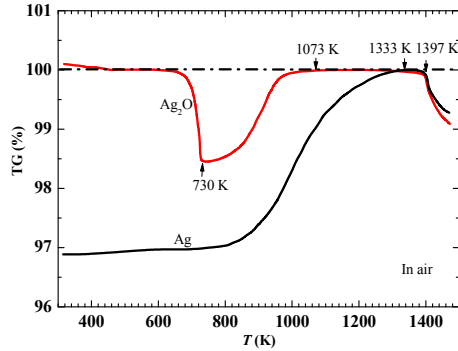
## 10 **2. $\text{AgNbO}_3$**

### 11 **2.1 Synthesis**

12 Both single crystal and ceramics of  $\text{AgNbO}_3$  are available. Single crystal can be grown by a  
13 molten salt method using  $\text{NaCl}$  or  $\text{V}_2\text{O}_5$  as a flux (Łukaszewski et al., 1980; Kania, 1989).  
14 Ceramics samples can be prepared through a solid state reaction between  $\text{Nb}_2\text{O}_5$  and silver  
15 source (Francombe & Lewis, 1958; Reisman & Holtzberg, 1958). Among the silver sources of  
16 metallic silver,  $\text{Ag}_2\text{O}$  and  $\text{Ag}_2\text{CO}_3$ ,  $\text{Ag}_2\text{O}$  is mostly proper to obtain single phase of  
17  $\text{AgNbO}_3$  (Valant et al., 2007b). For silver source of  $\text{Ag}_2\text{O}$ , thermogravimetric analysis  
18 indicates that phase formation can be reach at a firing temperature range of 1073-1397 K  
19 (Fig. 3). The issue frequently encountered in the synthesis of  $\text{AgNbO}_3$  is the decomposition  
20 of metallic silver, which can be easily justified from the color of the formed compounds.  
21 Pure powder is yellowish, and grey color of the powder generally indicates the presence of  
22 some metallic silver. It has been shown that the most important parameter that influences  
23 the phase formation is oxygen diffusion (Valant et al., 2007b). In our experiments to prepare  
24 the  $\text{AgNbO}_3$  ceramics, we first calcined the mixture of  $\text{Ag}_2\text{O}$  and  $\text{Nb}_2\text{O}_5$  at 1253 K for 6 hours  
25 in  $\text{O}_2$  atmosphere and then sintered the pellet samples for electric measurements at 1323 K  
26 for 6 hours in  $\text{O}_2$  atmosphere (Fu et al., 2007). Insulation of these samples is very excellent,  
27 which allows us to apply extremely high electric field to the sample (Breakdown field >220  
28 kV/cm. For comparison,  $\text{BaTiO}_3$  ceramics has a value of ~50 kV/cm.)

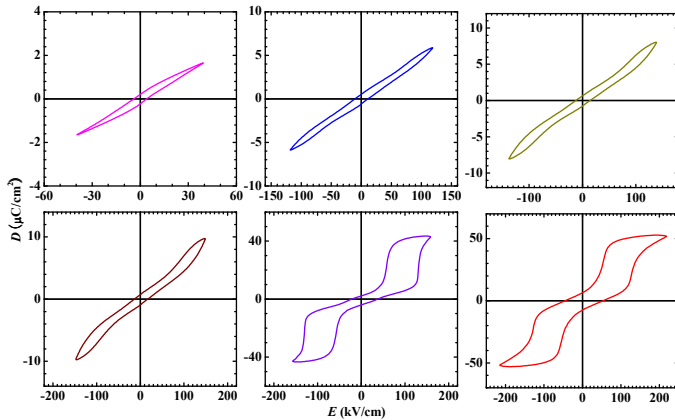
### 29 **2.2 Electric-field induced ferroelectric phase**

30 Previous measurements on  $D$ - $E$  hysteresis loop by Kania *et al.* (Kania et al., 1984) indicate  
31 that there is small spontaneous polarization  $P_s$  in the ceramics sample of  $\text{AgNbO}_3$ .  $P_s$  was  
32 estimated to be ~0.04  $\mu\text{C}/\text{cm}^2$  for an electric field with an amplitude of  $E=17$  kV/cm and a  
33 frequency of 60 Hz. Our results obtained at weak field have confirmed Kania's reports (Fig.  
34 4 and Fu et al., 2007). The presence of spontaneous polarization indicates that  $\text{AgNbO}_3$  must  
35 be ferroelectric at room temperature. The good insulation of our samples allows us to reveal  
36 a novel ferroelectric state at higher electric field. As shown in Fig.4, double hysteresis loop is  
37 distinguishable under the application of  $E\sim 120$  kV/cm, indicating the appearance of new  
38 ferroelectric phase. When  $E>150$  kV/cm, phase transformation is nearly completed and very  
39 large polarization was observed. At an electric field of  $E=220$  kV/cm, we obtained a value of  
40 52  $\mu\text{C}/\text{cm}^2$  for the ceramics sample. Associating with such structural change, there is very  
41 large electromechanical coupling in the crystal. The induced strain was estimated to be  
42 0.16% for the ceramics sample (Fig.5). The  $D$ - $E$  loop results unambiguously indicate that the  
43 atomic displacements are ordered in a *ferri*-electric way rather than an *anti-ferroelectric*  
44 way in the crystal at room temperature.



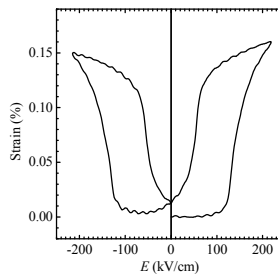
1  
2 Fig. 3. Thermogravimetric curves of the  $\text{AgNbO}_3$  formation in air using  $\text{Ag}_2\text{O}$  or metallic Ag  
3 powder as the silver source (Valant et al., 2007b). The curves are normalized to a weight of  
4 single-phase  $\text{AgNbO}_3$ . Temperatures of phase formation completed and decomposition are  
5 also indicated. For case of  $\text{Ag}_2\text{O}$ , decomposition of  $\text{Ag}_2\text{O}$  into Ag and oxygen occurs at  
6 temperature of  $\sim 730$  K.

7



8  
9 Fig. 4. D-E hysteresis loops for poly-crystalline  $\text{AgNbO}_3$  at room temperature.

10



11  
12 Fig. 5. Strain vs electric field for poly-crystalline  $\text{AgNbO}_3$  at room temperature.

### 2.3 Room-temperature structure

There are many works attempting to determine the room-temperature structure of  $\text{AgNbO}_3$  (Sciau et al., 2004; Francombe & Lewis, 1958; Verwerft et al., 1989; Fabry et al., 2000; Levin et al., 2009). However, none of these previous works can provide a *non-centrosymmetric* structure to reasonably explain the observed spontaneous polarization. Very recently, this longstanding issue has been addressed by R. Sano *et al.* (Sano et al., 2010). The space group of  $\text{AgNbO}_3$  has been unambiguously determined to be  $Pmc2_1$  (No. 26) by the convergent-beam electron diffraction (CBED) technique, which is *non-centrosymmetric* and allows the appearance of ferroelectricity in the crystal (Fig.6).

$Pmc2_1$ ( $T=298\text{K}$ )				
Site	$x$	$y$	$z$	$U$ ( $\text{\AA}^2$ )
Ag1 4c	0.7499(3)	0.7468(3)	0.2601(5)	0.0114(2)
Ag2	1/2	0.7466(6)	0.2379(5)	0.0114(2)
Ag3	0	0.7424(4)	0.2759(6)	0.0114(2)
Nb1	0.6252(2)	0.7525(5)	0.7332(2)	0.00389(18)
Nb2	0.1253(2)	0.24159	0.27981	0.00389(18)
O1 4c	0.7521(9)	0.7035(12)	0.7832(24)	0.0057(5)
O2 2b	1/2	0.804(3)	0.796(3)	0.0057(5)
O3 4c	0.6057(7)	0.5191(18)	0.4943(18)	0.0057(5)
O4 4c	0.6423(7)	0.0164(18)	0.539(2)	0.0057(5)
O5 2a	0	0.191(3)	0.256(3)	0.0057(5)
O6 4c	0.1339(9)	0.0410(17)	0.980(2)	0.0057(5)
O7 4c	0.1154(8)	0.4573(17)	0.5514(19)	0.0057(5)

Table 1. Structural parameters of  $\text{AgNbO}_3$  at  $T=298\text{K}$  (Yashima et al., 2011). Number of formula units of  $\text{AgNbO}_3$  in a unit cell:  $Z=8$ . Unit-cell parameters:  $a = 15.64773(3) \text{ \AA}$ ,  $b = 5.55199(1) \text{ \AA}$ ,  $c = 5.60908(1) \text{ \AA}$ ,  $\alpha = \beta = \gamma = 90 \text{ deg}$ ., Unit-cell volume:  $V = 487.2940(17) \text{ \AA}^3$ .  $U$  ( $\text{\AA}^2$ )=Isotropic atomic displacement parameter.

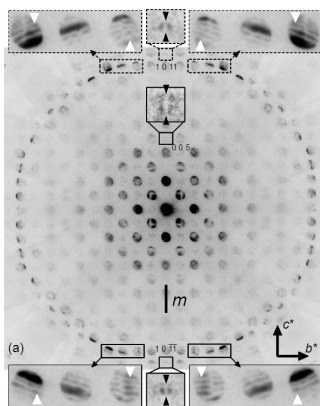


Fig. 6. Convergent-beam electron diffraction (CBED) pattern of  $\text{AgNbO}_3$  taken at the  $[100]$  incidence. In contrast to a mirror symmetry perpendicular to the  $b^*$ -axis, breaking of mirror symmetry perpendicular to the  $c^*$ -axis is seen, indicating that spontaneous polarization is along the  $c$ -direction (Taken by R. Sano & K. Tsuda (Sano et al., 2010)).

On the basis of this space group, M. Yashima (Yashima et al., 2011) exactly determined the atom positions (Table 1) in the structure using the neutron and synchrotron powder diffraction techniques. The atomic displacements are schematically shown in Fig.7. In contrast to the reported centrosymmetric  $Pbcm$  (Fabry et al. 2000; Sciau et al. 2004; Levin et al. 2009), in which the Ag and Nb atoms exhibit antiparallel displacements along the  $b$ -axis, the  $Pmc2_1$  structure shows a *ferri*-electric ordering of Ag and Nb displacements (Yashima et al., 2011) along the  $c$ -axis of  $Pmc2_1$  orthorhombic structure. This polar structure provides a reasonable interpretation for the observed polarization in  $AgNbO_3$ .

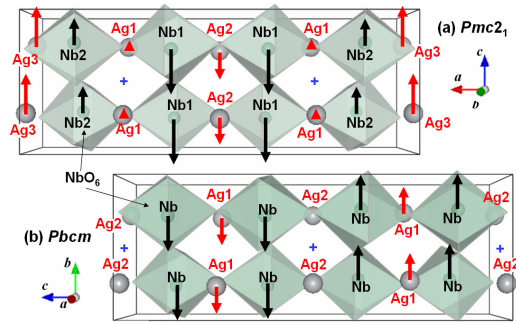


Fig. 7. (a) *Ferrielectric* crystal structure of  $AgNbO_3$  ( $Pmc2_1$ ) at room temperature. The atomic displacements along the  $c$ -axis lead to the spontaneous polarization in the crystal. (b) For comparison, the patterns for the previously reported  $Pbcm$  (Sciau et al., 2004) are also given. A cross (+) stands for the center of symmetry in the  $Pbcm$  structure. (by M. Yashima (Yashima et al., 2011)).

## 2.4 Dielectric behaviours and phase transitions

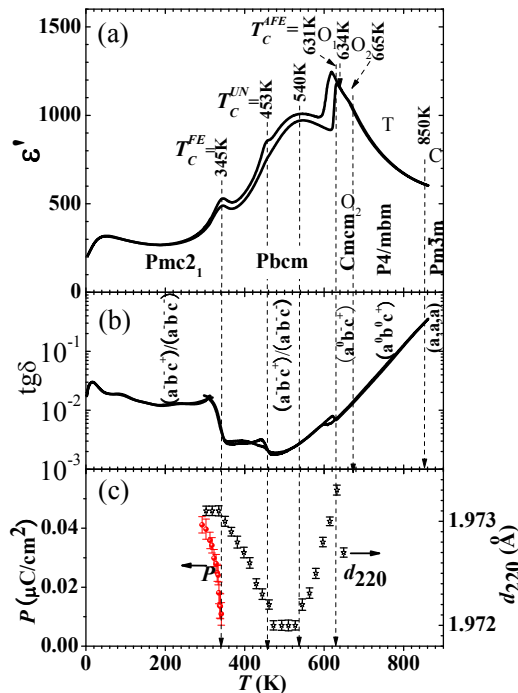
Initial works on the phase transitions of  $AgNbO_3$  and their influence on the dielectric behaviors were reported by Francombe and Lewis (Francombe & Lewis, 1958) in the late 1950s, which trigger latter intensive interests in this system (Łukaszewski et al., 1983; Kania, 1983, 1998; Kania et al., 1984, 1986; Pisarski & Dmytrow, 1987; Paweczyk, 1987; Hafid et al., 1992; Petzelt et al., 1999; Ratuszna et al., 2003; Sciau et al., 2004). The phase transitions of  $AgNbO_3$  were associated with two mechanisms of *displacive* phase transition: tilting of oxygen octahedra and displacements of particular ions (Sciau et al., 2004). Due to these two mechanisms, a series of structural phase transitions are observed in  $AgNbO_3$ . The results on dielectric behaviors together with the reported phase transitions are summarized in Fig.8. Briefly speaking, the structures of the room-temperature (Yashima et al., 2011) and the high temperature phases ( $T > T^{O1-O2}=634$  K) (Sciau et al., 2004) are exactly determined, in contrast, those of low-temperature ( $T < \text{room temperature}$ ) and intermediate phases ( $T_C^{FE}=345$  K  $< T < T^{O1-O2}$ ) remain to be clarified. In the dielectric curve, we can see a shoulder around 40 K. It is unknown whether this anomaly is related to a phase transition or not. It should be noticed that Shigemi *et al.* predicted a ground state of  $R3c$  rhombohedra phase similar to that of  $NaNbO_3$  for  $AgNbO_3$  (Shigemi & Wada, 2008). Upon heating, there is an anomaly at  $T_C^{FE}=345$  K, above which spontaneous polarization was reported to disappear (Fig.8 (c) and Kania et al., 1984). At the same temperature, anomaly of lattice distortion was observed (Fig.8 (c) and Levin et al., 2009). The dielectric anomaly at  $T_C^{FE}=345$  K was attributed to be a ferroelectric phase transition. Upon further heating, there is a small peak at  $T=453$  K, which

		AgNbO <sub>3</sub>			
Atom		573 K	645 K	733 K	903 K
Nb	<i>x</i>	0.2460(15)	1/4	0	0
	<i>y</i>	0.2422(10)	1/4	0	0
	<i>z</i>	0.1256(6)	0	0	0
Ag(1)	<i>U</i> (Å <sup>2</sup> )	1.12(6)	1.31(4)	1.38(4)	1.63(2)
	<i>x</i>	-0.2507(35)	0	0	1/2
	<i>y</i>	1/4	-0.001(2)	1/2	1/2
	<i>z</i>	0	1/4	1/2	1/2
Ag(2)	<i>U</i> (Å <sup>2</sup> )	2.78(7)	1.98(6)	2.80(3)	3.47(4)
	<i>x</i>	-0.2556(26)	0		
	<i>y</i>	0.2428(18)	0.494(3)		
	<i>z</i>	1/4	1/4		
O(1)	<i>U</i> (Å <sup>2</sup> )	1.73(6)	3.54(8)		
	<i>x</i>	0.3022	0.2827(7)	0	0
	<i>y</i>	1/4	1/4	0	0
O(2)	<i>z</i>	0	0	1/2	1/2
	<i>U</i> (Å <sup>2</sup> )	1.31(6)	2.27(5)	3.14(5)	3.60(4)
	<i>x</i>	-0.0292(14)	0	0.2782(3)	
	<i>y</i>	0.0303(14)	0.2259(8)	0.2218	
O(3)	<i>z</i>	0.1140(6)	0.0205(8)	0.0358(4)	
	<i>U</i> (Å <sup>2</sup> )	1.71(7)	1.94(4)	2.08(4)	
	<i>x</i>	0.5262(13)	0.2710(7)		
	<i>y</i>	0.4778(14)	0.2456(11)		
O(4)	<i>z</i>	0.1375(5)	1/4		
	<i>U</i> (Å <sup>2</sup> )	1.17(6)	2.56(6)		
	<i>x</i>	0.2155(23)			
	<i>y</i>	0.2622(24)			
cell	<i>z</i>	1/4			
	<i>U</i> (Å <sup>2</sup> )	1.67(7)			
	<i>a</i> (Å)	5.5579(5)	7.883(1)	5.5815(3)	3.9598(3)
	<i>b</i> (Å)	5.5917(6)	7.890(1)		
	<i>c</i> (Å)	15.771(2)	7.906(1)	3.9595(3)	

Table 2. Structural parameters for high temperature phases at 573 K(*Pbcm*), 645 K(*Cmcm*), 733 K (*P4/mbm*), and 903 K(*Pm3m*) (Sciau et al., 2004).

is not so visible. However, it can be easily ascertained in the differential curve or in the cooling curve. This anomaly is nearly unnoticed in the literatures (Łukaszewski et al., 1983; Kania, 1983, 1998; Kania et al., 1986; Pisarski & Dmytrow, 1987; Paweczyk, 1987; Hafid et al., 1992; Ratuszna et al., 2003). The detailed examination of the temperature dependence of the 220<sub>o</sub> *d*-spacing (reflection was indexed with orthorhombic structure) determined by Levin *et al.* (Levin et al., 2009 and Fig.8(c)) reveals anomaly that can be associated with this dielectric peak. These facts suggest that a phase transition possibly occurs at this temperature. Around 540 K, there is a broad and frequency-dependent peak of dielectric constant, which is also associated with an anomaly of 220<sub>o</sub> *d*-spacing. However, current structural investigations using x-ray and neutron diffraction do not find any symmetric changes associated with the

1 dielectric anomalies at 456 K and 540 K, and the structure within this intermediate  
 2 temperature range was assumed to be orthorhombic  $Pbcm$  (Sciau et al., 2004). At  
 3  $T=T_C^{AFE}=631$  K, there is a sharp jump of dielectric constant due to an antiferroelectric phase  
 4 transition (Pisarski et al., 1987; Sciau et al., 2004). The atomic displacement patterns in the  
 5 antiferroelectric phase ( $Pbcm$ ) are shown in Fig.7 (b) using the structural parameters  
 6 determined by Ph Sciau *et al.* (Sciau et al., 2004). For  $T>T_C^{AFE}$ , there are still three phase  
 7 transitions that are essentially derived by the tilting of oxygen octahedral and have only  
 8 slight influence on the dielectric constant. For conveniences, the tilting of octahedral (Sciau  
 9 et al., 2004) described in Glazer's notation is given in Fig.8 and the structure parameters  
 10 (Sciau et al., 2004) are relisted in Table 2.  
 11



12  
 13 Fig. 8. Temperature dependence of (a) dielectric constant, (b) dielectric loss, and (c)  
 14 polarization (Kania et al., 1984) and  $220_O$   $d$ -spacing of the lattice (Levin et al., 2009).

### 15 3. ( $Ag_{1-x}Li_x$ ) $NbO_3$ solid solution

16 Li can be incorporated into the Ag-site of  $AgNbO_3$ . However, due to the large difference of  
 17 ionic radius of  $Li^+(0.92\text{\AA})$ , and  $Ag^+(1.28\text{\AA})$  (Shannon, 1976), the solid solution is very  
 18 limited. Nalbandyan *et al.* (Nalbandyan et al., 1980), systematically studied the stable and  
 19 metastable phase equilibria and showed that solid solution limit is narrow ( $x \sim 0.02$ ) for the  
 20 stable phase, but is relatively wide ( $x \sim 0.12$ ) for the metastable phase (Sakabe et al., 2001;

1 Takeda et al., 2003; Fu et al., 2008, 2011). With a small substitution of Li for Ag  
 2 ( $x > x_c = 0.05 \sim 0.06$ ), a ferroelectric rhombohedra phase is evolved in the solid solution  
 3 (Nalbandyan et al., 1980; Sakabe et al., 2001; Takeda et al., 2003; Fu et al., 2008, 2011). In this  
 4 solid solution, the strong off-center of small Li (Bilc & Singh, 2006) plays an important role  
 5 in triggering the ferroelectric state with large spontaneous polarization (Fu et al., 2008, 2011).

### 6 3.1 Synthesis

7 Single crystals of  $(\text{Ag}_{1-x}\text{Li}_x)\text{NbO}_3$  can be obtained by the melt growth process (Fu et al.,  
 8 2008). Stoichiometric compositions of  $\text{Ag}_2\text{O}$ ,  $\text{Li}_2\text{CO}_3$ , and  $\text{Nb}_2\text{O}_5$  were mixed and calcined at  
 9 1253 K for 6 h in an oxygen atmosphere. The calcined powder was milled, put into an  
 10 alumina container, and melted at 1423 K for 4 h in an oxygen atmosphere. The melt was  
 11 cooled to 1323 K to form the crystal at a rate of 4 K/h, followed by furnace cooling down to  
 12 room temperature. Using this process, single crystals with size of 1–3 cm can be obtained for  
 13 the  $(100)_p$  (Hereafter, subscript  $p$  indicates pseudocubic structure) growth face. Due to the  
 14 volatility of lithium at high temperature, the exact chemical composition of the crystal is  
 15 generally deviated from the starting composition and is required to be determined with  
 16 methods like inductively coupled plasma spectrometry.

17 Ceramics samples can be prepared by a solid state reaction approach. Mixtures of  $\text{Ag}_2\text{O}$ ,  
 18  $\text{Nb}_2\text{O}_5$ , and  $\text{Li}_2\text{CO}_3$  were calcined at 1253 K for 6 h in  $\text{O}_2$  atmosphere, followed by removal of  
 19 the powder from the furnace to allow a rapid cooling to prevent phase separation. The  
 20 calcined powder was milled again and pressed to form pellets that were sintered at 1323 K  
 21 for 6 h in  $\text{O}_2$  atmosphere, followed by a rapid cooling.

### 22 3.2 Structure

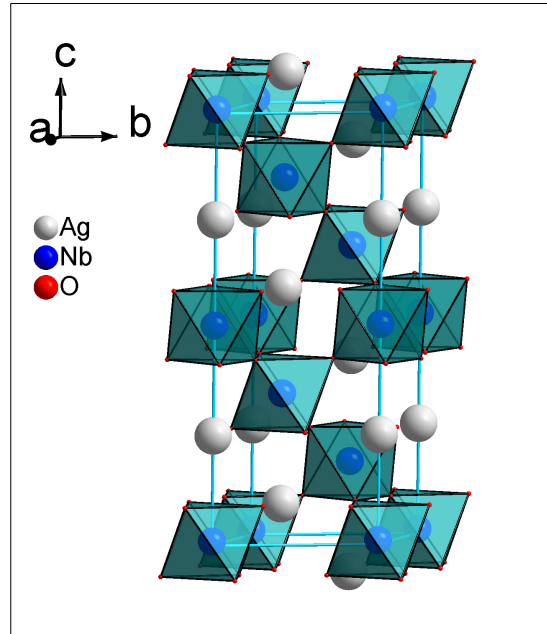
23 The structural refinements using the powder X-ray diffraction data suggest that  $(\text{Ag}_{1-x}\text{Li}_x)\text{NbO}_3$   
 24 solid solution with  $x > x_c$  has the space group of  $R3c$  (Fu et al., 2011). Table 3 lists  
 25 the structural parameters of this model for composition  $x=0.1$ . Figure 9 shows a schematic  
 26 drawing for this structure. In this rhombohedral  $R3c$  phase, the spontaneous polarization is  
 27 essentially due to the atomic displacements of the Ag/Li, Nb, and O atoms along the  
 28 pseudocubic [111] direction.

$\text{Ag}_{0.9}\text{Li}_{0.1}\text{NbO}_3$ ( $R3c$ , No.161, $T=\text{room temperature}$ )					
$a(\text{\AA})$	5.520		$\alpha$	90	
$b(\text{\AA})$	5.520		$\beta$	90	
$c(\text{\AA})$	13.79		$\gamma$	120	
$V(\text{\AA}^3)$	364.0				
Atom	Site	$x$	$y$	$z$	$U(\text{\AA}^2)$
Ag/Li	6a	0	0	0.2545(8)	0.5
Nb	6a	0	0	0.0097(8)	0.5
O	18b	0.5533	1	0.2599(9)	0.5

30 Table 3. Structural parameters for rhombohedra structure of  $(\text{Ag,Li})\text{NbO}_3$  solid solution.

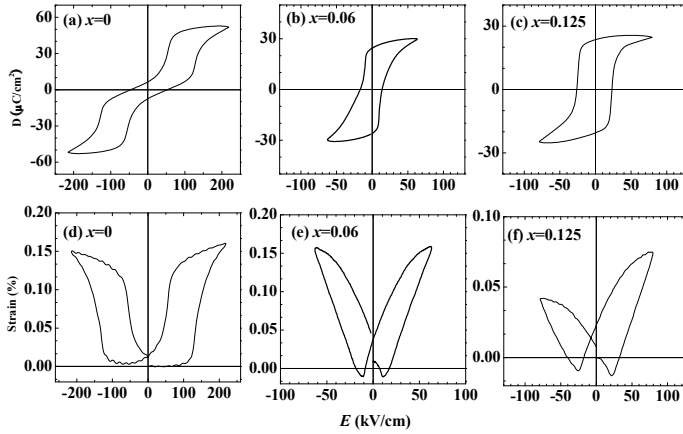
### 31 3.3 Ferroelectric and piezoelectric properties

32 Evolution of the polarization state in  $\text{Ag}_{1-x}\text{Li}_x\text{NbO}_3$  solid solutions is shown in Fig.10.  
 33 Basically, when  $x < x_c$ , the solid solutions have the *ferrielectric* state of pure  $\text{AgNbO}_3$  with a  
 34 small spontaneous polarization at zero electric field. In contrast, when  $x > x_c$ , a normal

1  
23  
45 Fig. 9. Schematic structure of  $\text{Ag}_{1-x}\text{Li}_x\text{NbO}_3$  ( $x = 0.1$ ) with symmetry  $R3c$  (No.161).

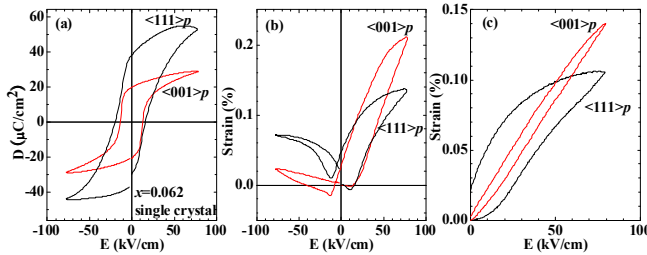
6 ferroelectric state with large value of remanent polarization ( $P_r$ ) is observed. All ceramics  
 7 samples show  $P_r$  value comparable to  $P_5$  of  $\text{BaTiO}_3$  single crystal ( $26 \mu\text{C}/\text{cm}^2$ ) (Shiozaki et  
 8 al., 2001). Moreover, the polarization in  $\text{Ag}_{1-x}\text{Li}_x\text{NbO}_3$  solid solution is very stable after  
 9 switching. Large  $P_r$  value and ideal bistable polarization state of  $\text{Ag}_{1-x}\text{Li}_x\text{NbO}_3$  ceramics may  
 10 be interesting for non-volatile ferroelectric memory applications. Measurements on single  
 11 crystal samples (Fig.11) indicate that saturation polarization along the  $\langle 111 \rangle_p$  rhombohedra  
 12 direction ( $P_s^{\langle 111 \rangle} \sim 40 \mu\text{C}/\text{cm}^2$ ) is greatly larger than that along the  $\langle 001 \rangle_p$  tetragonal  
 13 direction ( $P_s^{\langle 001 \rangle} \sim 24 \mu\text{C}/\text{cm}^2$ ) and the ratio between them is  $\sqrt{3}$  (Fu et al., 2008), which is in  
 14 good agreement with results of structural refinements. This suggests that the polar axis is  
 15 the  $\langle 111 \rangle_p$  direction of pseudo-cubic structure.

16 The strain- $E$  loops indicate that there are good electromechanical coupling effects in  $\text{Ag}_{1-}$   
 17  $x\text{Li}_x\text{NbO}_3$  crystals. Although the spontaneous polarization is along the  $\langle 111 \rangle_p$  axis, the  
 18  $\langle 001 \rangle_p$ -cut crystal shows larger strain and less hysteresis than the  $\langle 111 \rangle_p$ -cut one (Fig.11 (b)  
 19 and (c)). These phenomena are very similar to those reported for the relaxor-ferroelectric  
 20 crystals (Wada et al., 1998). The most significant result exhibited from  $\text{Ag}_{1-x}\text{Li}_x\text{NbO}_3$  single  
 21 crystal is its excellent  $g_{33}$  value that determines the voltage output of the piezoelectric device  
 22 under the application of an external stress (Fu et al., 2008). The  $g_{33}$  value together the  $d_{33}$   
 23 value and dielectric constants for the  $\langle 001 \rangle_p$ -cut single crystals are shown in Fig. 12. The  
 24 high  $g_{33}$  value is a direct result from the large  $d_{33}$  constant and the low dielectric constant of  
 25 the single crystal.



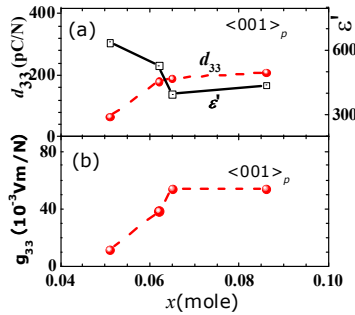
1  
2  
3

Fig. 10. Typical  $D$ - $E$  and strain- $E$  loops for the  $\text{Ag}_{1-x}\text{Li}_x\text{NbO}_3$  ceramics samples.



4  
5  
6  
7

Fig. 11. (a)  $D$ - $E$  loops, (b) strain vs  $E$  for bipolar electric field, and (c) strain vs  $E$  for unipolar field for  $\text{Ag}_{1-x}\text{Li}_x\text{NbO}_3$  single crystal with  $x=0.062$ .



8  
9  
10

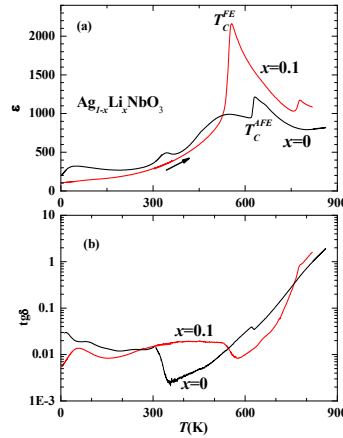
Fig. 12. Composition dependence of dielectric constant  $\epsilon$ ,  $d_{33}$  and  $g_{33}$  for the  $\langle 001 \rangle_p$ -cut  $\text{Ag}_{1-x}\text{Li}_x\text{NbO}_3$  single crystals.

### 3.4 Dielectric behaviours and proposed phase diagram

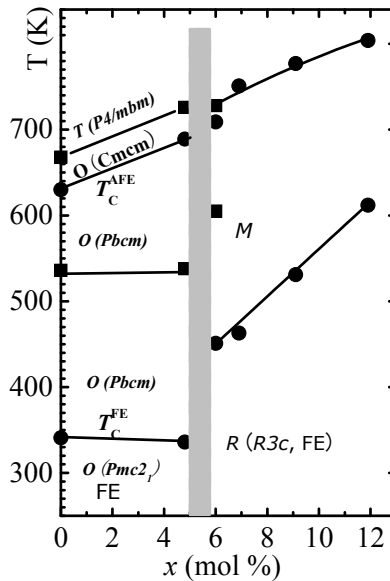
11  
12  
13

Figure 13 shows the dielectric behaviours of the ferroelectric  $\text{Ag}_{1-x}\text{Li}_x\text{NbO}_3$  solid solutions. For comparison, the temperature dependence of dielectric constant of  $\text{AgNbO}_3$  is also

1 shown. It can be seen that solid solution with  $x > x_c$  shows different temperature evolutions  
 2 of the dielectric constant as compared with  $\text{AgNbO}_3$ . In sharp contrast to the complex  
 3 successive phase transitions in  $\text{AgNbO}_3$ , ferroelectric  $\text{Ag}_{1-x}\text{Li}_x\text{NbO}_3$  solid solutions ( $x > x_c$ )  
 4 show only two phase transitions in the temperature range of 0-820 K. Polarization  
 5 measurements suggest that the high temperature phase ( $T > T_C^{\text{FE}}$ ) is nonpolar, thus it seems  
 6



7  
 8 Fig. 13. Typical dielectric behaviours of  $\text{Ag}_{1-x}\text{Li}_x\text{NbO}_3$  ceramics in comparison with that of  
 9 pure  $\text{AgNbO}_3$ .



11  
 12 Fig. 14. Phase diagram proposed for  $\text{Ag}_{1-x}\text{Li}_x\text{NbO}_3$  solid solution. The gray area indicates  
 13 the phase boundary (Fu et al., 2011).

1 that the higher temperature phase transition is not related to a ferroelectric phase transition.  
 2 On the basis of the dielectric measurements, the phase diagram of  $\text{Ag}_{1-x}\text{Li}_x\text{NbO}_3$  solution is  
 3 summarized in Fig.14, where  $T$ ,  $O$ ,  $R$  and  $M$  represent tetragonal, orthorhombic,  
 4 rhombohedra, and monoclinic symmetries, respectively. At room temperature, structure  
 5 transformation from  $O$  to  $R$  phase at  $x_c$  dramatically changes the polar nature of  $\text{Ag}_{1-}$   
 6  $x\text{Li}_x\text{NbO}_3$ . It is a *ferrielectric* with small spontaneous polarization in the  $O$  phase, but  
 7 becomes a ferroelectric with large polarization in the  $R$  phase.

#### 8 **4. ( $\text{Ag}_{1-x}\text{Na}_x$ ) $\text{NbO}_3$ solid solution**

9 The ionic radius of  $\text{Na}^+$  (1.18 Å) is comparable to that of  $\text{Ag}^+$  (1.28 Å) (Shannon, 1976),  
 10 allowing to prepare the  $\text{Ag}_{1-x}\text{Na}_x\text{NbO}_3$  solid solution within the whole range of composition  
 11 ( $x=0-1$ ) (Kania & Kwapulinski, 1999). Kania *et al.* previously performed investigation on the  
 12 dielectric behaviors and the differential thermal analysis for the  $\text{Ag}_{1-x}\text{Na}_x\text{NbO}_3$  solid  
 13 solutions, and stated that the solid solution evolves from disordered antiferroelectric  
 14  $\text{AgNbO}_3$  to normal antiferroelectric  $\text{NaNbO}_3$ . As described in section §2.3, we now know  
 15 that  $\text{AgNbO}_3$  is not *antiferroelectric* but rather is *ferrielectric* at room temperature (Yashima *et*  
 16 *al.*, 2011). Moreover, recent reexamination on the polarization behaviors of stoichiometric  
 17 and non-stoichiometric  $\text{NaNbO}_3$  polycrystallines indicates that the reported clamping  
 18 hysteresis loop of  $\text{NaNbO}_3$  can be interpreted by pinning effects while stoichiometric  
 19  $\text{NaNbO}_3$  is intrinsically *ferroelectric* (Arioka *et al.*, 2010). Therefore, reexamination on this  
 20 solid solution is necessary. Evolution of the polarization with composition clearly indicates  
 21 that the solid solution evolves from *ferrielectric*  $\text{AgNbO}_3$  to *ferroelectric*  $\text{NaNbO}_3$ .

#### 22 **4.1 Synthesis**

23  $\text{Ag}_{1-x}\text{Na}_x\text{NbO}_3$  solid solution was prepared by a solid state reaction approach. Mixtures of  
 24  $\text{Ag}_2\text{O}$ (99%),  $\text{Nb}_2\text{O}_5$  (99.99%), and  $\text{Na}_2\text{CO}_3$  (99.99%) were calcined at 1173 K for 4 h in  $\text{O}_2$   
 25 atmosphere. The calcined powder was ground, pressed into pellet with a diameter of 10 mm  
 26 at thickness of 2 mm, and sintered with the conditions listed in Table 4.  
 27

Composition	Temperature	Time	atmosphere
$x=0,0.1,0.2$	1273K	5h	$\text{O}_2$
$x=0.4, 0.5, 0.6$	1323K	5h	$\text{O}_2$
$x= 0.8,0.9,1$	1373K	5h	$\text{O}_2$

28 Table 4. Sintering conditions for  $\text{Ag}_{1-x}\text{Na}_x\text{NbO}_3$ .

#### 29 **4.2 Polarization**

30 Figure 15 shows the change in polarization with composition in the  $\text{Ag}_{1-x}\text{Na}_x\text{NbO}_3$  solid  
 31 solutions. For a wide range of composition  $x<0.8$ , the solid solution possesses the  
 32 characteristic polarization behaviours of pure  $\text{AgNbO}_3$ : small spontaneous polarization at  
 33  $E=0$  but large polarization at  $E>$  a critical field. This fact suggests that the solid solution is  
 34 *ferrielectric* within this composition range. This is also supported by the temperature  
 35 dependence of dielectric constant (Fig.16). On the other hand, for the Na-rich composition,

1 particularly,  $x > 0.8$ , we observed large remanent polarization with value close to the  
2 saturation polarization at high field. This result indicates that a normal ferroelectric phase is  
3 stable in these compositions. Therefore, polarization measurements show that the  $\text{Ag}_{1-x}\text{Na}_x\text{NbO}_3$   
4 solid solution evolves from *ferrielectric*  $\text{AgNbO}_3$  to *ferroelectric*  $\text{NaNbO}_3$ .

### 5 4.3 Dielectric properties

6 The dielectric properties of the  $\text{Ag}_{1-x}\text{Na}_x\text{NbO}_3$  solid solutions are summarized in Fig.16. The  
7 change in dielectric behaviours with composition is very similar to that observed in  
8 polarization measurements (Fig.15). For  $x \leq 0.8$ , the solid solution shows successive phase  
9 transitions similar to pure  $\text{AgNbO}_3$ . In contrast, it has the characteristic phase transition of  
10 pure  $\text{NaNbO}_3$  for  $x > 0.8$ . The composition dependence of transition temperature derived  
11 from the dielectric measurements is shown in Fig.17. Two noticed features may be seen: (a)  
12 the thermal hysteresis is extremely large for antiferroelectric phase transition and reaches a  
13 value greater than 100 K at  $x \sim 0.5$ . Such large thermal hysteresis is rarely observed in normal  
14 polar phase transition. (b) It seems that there is a phase boundary within  $x = 0.8-0.9$ , around  
15 which structural transformation between *ferri-* and *ferro-*electric phases occurs.

## 16 5. ( $\text{Ag}_{1-x}\text{K}_x$ ) $\text{NbO}_3$ solid solution

17 ( $\text{Ag}_{1-x}\text{K}_x$ ) $\text{NbO}_3$  solid solutions are available only for very limited composition (Weirauch &  
18 Tennery, 1967; Łukaszewski, 1983; Kania, 2001). Weirauch *et al.* reported that solid solution  
19 of  $\text{AgNbO}_3$  in  $\text{KNbO}_3$  was limited to slightly less than 6 mole % and solid solution of  $\text{KNbO}_3$   
20 in  $\text{AgNbO}_3$  was limited to less than 0.5 mole % (Weirauch & Tennery, 1967). However, our  
21 process indicates that  $\text{KNbO}_3$  and  $\text{AgNbO}_3$  can be alloyed with each other within 20 mole %  
22 (Fu *et al.*, 2009a). Apparently, the reported solid solution limit is dependent on the process.  
23 In our samples, we found that a ferroelectric phase with large spontaneous polarization can  
24 be induced by substitution of Ag with K for  $x > x_{c1} = 0.07$ . This ferroelectric phase shows  
25 nearly composition-independent ferroelectric phase transition. On the other hand, the K-rich  
26 solid solution ( $x > 0.8$ ) possesses the ferroelectric phase transition sequence of pure  $\text{KNbO}_3$   
27 and the transition temperature is dependent on the composition.

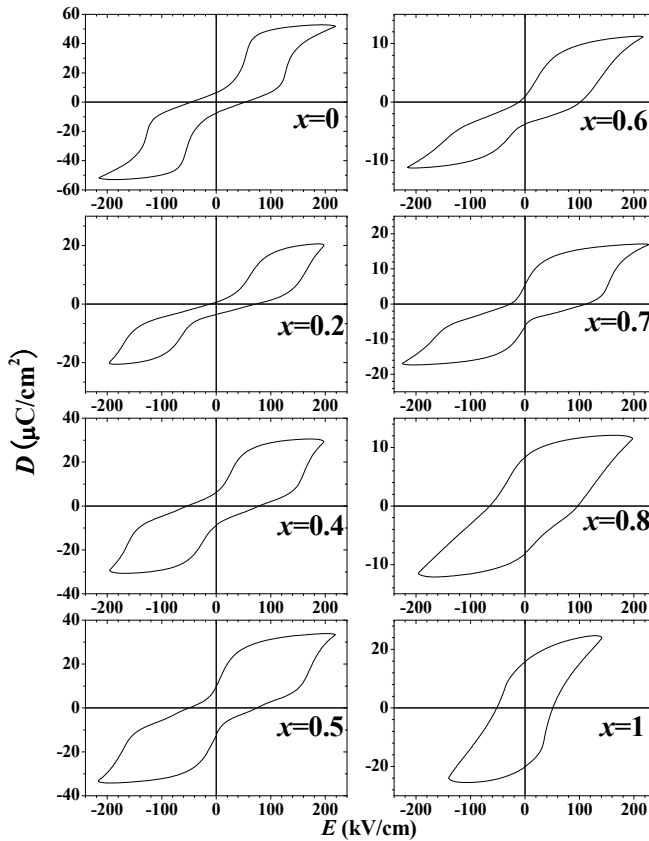
### 28 5.1 Synthesis

29 ( $\text{Ag}_{1-x}\text{K}_x$ ) $\text{NbO}_3$  solid solutions were prepared by a solid state reaction method. Mixture of  
30  $\text{Ag}_2\text{O}$ ,  $\text{Nb}_2\text{O}_5$ , and  $\text{K}_2\text{CO}_3$  were calcined at 1173 K for 6 h in  $\text{O}_2$  atmosphere with a slow  
31 heating rate of 1 K/min. The calcined powder was milled again, pressed in a 6-mm steel die  
32 with a pressure of 10 MPa to form the pellets, which were then preheated at 773 K for 2 h,  
33 followed by a sintering at temperature of 1253–1323 K (1323 K for  $x = 0-0.1$  and 1.00, 1273 K  
34 for  $x = 0.15$  and 0.90, and 1253 K for  $x = 0.17$  and 0.80, respectively) for 3 h in  $\text{O}_2$  atmosphere.  
35 The atmosphere and heating rate are found to have significant influences on the phase  
36 stability of the solid solution.

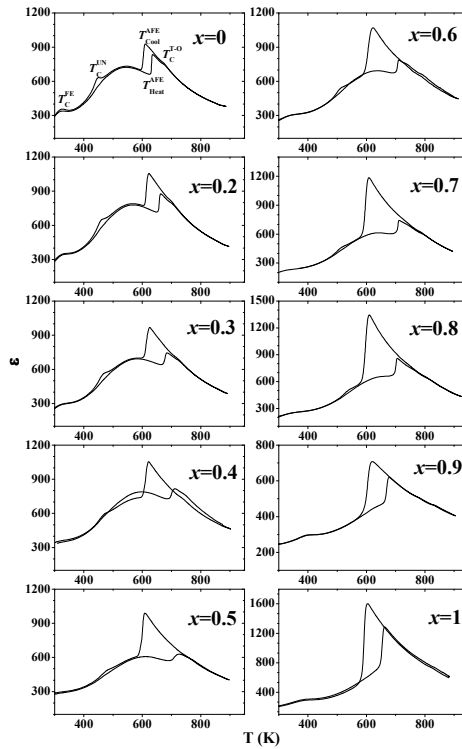
### 37 5.2 Structural change with composition

38 Figure 18 shows the change in lattice parameters with composition in the  $\text{Ag}_{1-x}\text{K}_x\text{NbO}_3$  solid  
39 solutions. When the amount of substitution is small, the solid solution possesses the  
40 orthorhombic structure of pure  $\text{AgNbO}_3$ . In the phase boundary  $x_{c1} = 0.07$ , structural  
41 transformation occurs and the phase changes into a new orthorhombic structure. In this new

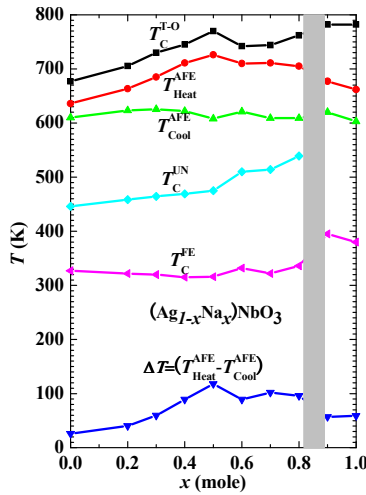
1 ferroelectric phase, the lattice constants show linear increase with composition.  
 2 Interestingly, the orthorhombic distortion angle  $\beta$  is nearly independent with the  
 3 composition. In the K-rich region ( $x > x_{c3} = 0.8$ ), the solid solution has the orthorhombic  
 4 structure of pure  $\text{KNbO}_3$  at room-temperature, which is also ferroelectric. In contrast to  
 5 nearly unchanged orthorhombic angle  $\beta$  in the Ag-rich orthorhombic phase,  $\beta$  shows  
 6 monotonous decreases with  $x$  in the K-rich phase.  
 7  
 8  
 9  
 10  
 11  
 12



13  
 14  
 15  
 16  
 17 Fig. 15. Composition dependence of  $D$ - $E$  loops obtained at room temperature for  $\text{Ag}_{1-x}\text{Na}_x\text{NbO}_3$  solid solutions  
 18



1  
2 Fig. 16. Temperature dependence of dielectric constants for  $\text{Ag}_{1-x}\text{Na}_x\text{NbO}_3$  solid solutions.  
3



4  
5 Fig. 17. Composition dependence of phase transition temperatures detected from dielectric  
6 measurements for  $\text{Ag}_{1-x}\text{Na}_x\text{NbO}_3$  solid solutions.

**5. 3 Ferroelectric and piezoelectric properties**

Figure 19 shows typical results of polarization and strain behaviors observed at room temperature for the  $Ag_{1-x}K_xNbO_3$  solid solutions. Similar to pure  $AgNbO_3$ , merely a small spontaneous polarization was observed in samples with  $x < x_{c1}$ . However, when  $x > x_{c1}$ , a normal  $D-E$  loop with large value of remanent polarization  $P_r$  was observed. A value of  $P_r=20.5 \mu C/cm^2$  was obtained for a ceramics sample with  $x =0.10$ , which is greatly larger than that observed for  $BaTiO_3$  ceramics (Fu et al., 2010). These results show that Ag-rich orthorhombic phase ( $x_{c1} < x < x_{c2}$ ) is really under a ferroelectric state with large polarization. For K-rich region  $x > x_{c3}$ , normal  $D-E$  loops were also obtained. Associating with the evolution into the ferroelectric phase, butterfly strain curve were observed. The piezoelectric constants determined from the piezo- $d_{33}$  meter generally have value of 46–64 pC/N for these ferroelectric samples (Fu et al., 2009a).

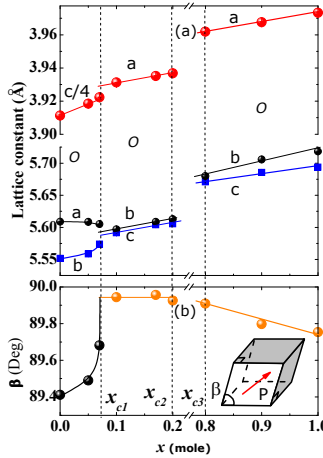


Fig. 18. Lattice parameters change with composition in  $Ag_{1-x}K_xNbO_3$  solid solution.  $\beta$  is the orthorhombic distortion angle. The inset shows the orthorhombic distortion due to the ferroelectric displacements along the  $\langle 110 \rangle_p$  direction of the pseudocubic structure.

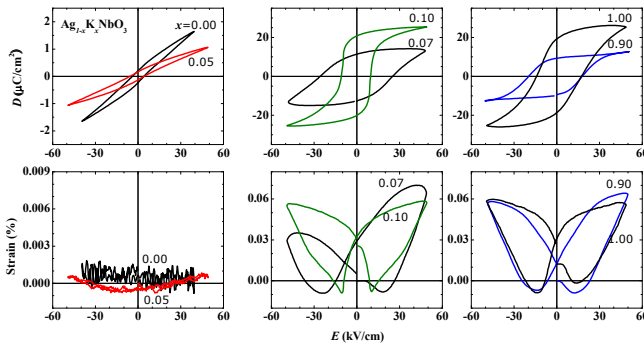


Fig. 19. Changes of polarization and strain under the application of electric field with composition at room temperature.

#### 5.4 Dielectric behaviours and proposed phase diagram

Associating with the change in structure, dielectric behaviours of the  $\text{Ag}_{1-x}\text{K}_x\text{NbO}_3$  solid solution also change with composition. As shown in Fig.20, the temperature dependence of dielectric constant can be sorted by three types: (1)  $\text{AgNbO}_3$ -type for  $x < x_{c1} = 0.07$ , (2)  $\text{KNbO}_3$ -type for K-rich region  $x > x_{c3} = 0.8$ , and (3) a new type for the intermediate composition  $x_{c1} < x < x_{c2}$ . In this intermediate composition, dielectric measurements indicate that there are two phase transitions within the temperature range of 0-750 K. One transition locates at  $T_{c2} \sim 420$  K with thermal hysteresis and shows small change in dielectric constant, which seems to be due to a ferro-to-ferro-electric phase transition. Another phase transition occurs at  $T_{c1} \sim 525$  K. Around this transition, the dielectric constant changes sharply and follows exactly the Curie-Weiss law. The Curie-Weiss constant was estimated to be  $1.47 \times 10^5$  K for  $x = 0.1$  sample, which is a typical value for the displacive ferroelectric transition, suggesting that this is a displacive type ferroelectric transition. A phase diagram is proposed in Fig.21, in which PE, FE, and AFE represent the paraelectric, ferroelectric, and antiferroelectric phases, respectively. When carefully comparing the phase transition temperature with the orthorhombic angle  $\beta$  (Fig.18) due to the ferroelectric distortion (For  $x_{c1} < x < x_{c2}$  and  $x > x_{c3}$ . In contrast, for  $x < x_{c1}$ ,  $\beta$  change is basically due to the oxygen-octahedral tilting.), one might find that there is a correlation between  $\beta$  and the temperature of the ferroelectric phase transition.

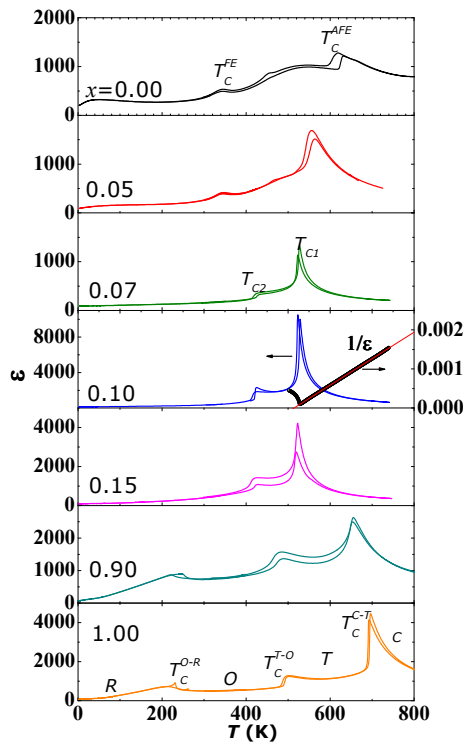


Fig. 20. Temperature dependence of dielectric constant for  $\text{Ag}_{1-x}\text{K}_x\text{NbO}_3$  solid solution.

## 6. AgTaO<sub>3</sub>

AgTaO<sub>3</sub> is another oxide of the two discovered silver perovskites (Francombe & Lewis, 1958). It is generally accepted that AgTaO<sub>3</sub> undergoes a series of phase transitions from rhombohedral phase ( $T \leq 685$  K) to monoclinic phase ( $650 \text{ K} \leq T \leq 703$  K) and then to tetragonal phase ( $685 \text{ K} < T \leq 780$  K), and finally to cubic phase at  $T_{T-C} = 780$  K upon heating (Francombe & Lewis, 1958; Kania, 1983; Paweczyk, 1987; Kugel et al., 1987; Hafid et al., 1992). However, due to the coexistence regions between rhombohedral and monoclinic, and monoclinic and tetragonal, the actual transition temperatures from rhombohedral to monoclinic  $T_{R-M}$  as well as that from monoclinic to tetragonal  $T_{M-T}$  still remain uncertain. Furthermore, the ground state and the origins that trigger these phase transitions still remain to be addressed (Soon et al., 2010; Kugel et al., 1987; Wołczyr & Łukaszewski, 1986).

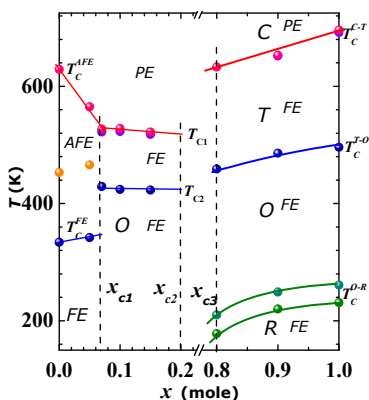
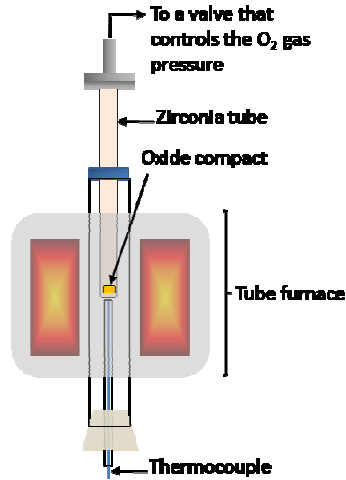


Fig. 21. Phase diagram proposed for the Ag<sub>1-x</sub>K<sub>x</sub>NbO<sub>3</sub> solid solution. Phase boundaries are indicated by the dashed lines. C, T, O, and R indicate the cubic, tetragonal, orthorhombic, and rhombohedral symmetries, respectively. PE, FE and AFE represent paraelectric, ferroelectric, and antiferroelectric phases, respectively.

### 6.1 Synthesis

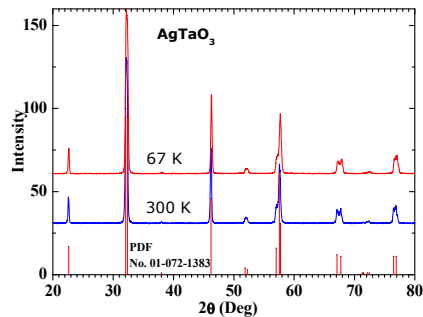
Although single crystal of AgTaO<sub>3</sub> is available through a flux method (Łukaszewski et al., 1980; Kania, 1989), it is extremely difficult to prepare its dense ceramics sample (Francombe & Lewis, 1958; Kania, 1983) for electrical measurements. Since decomposition of AgTaO<sub>3</sub> occurs at  $1443 \pm 3$  K in atmosphere (Valant et al., 2007b), sintering cannot be performed at higher temperatures to obtain dense ceramics. However, this long-standing synthesis difficulty now can be solved by a processing route involving the conventional solid-state reaction and sintering in environment with a high oxygen pressure at  $\sim 13$  atm (Soon et al., 2010). In this synthesizing route, Ag<sub>2</sub>O and Ta<sub>2</sub>O<sub>5</sub>, first underwent a grind mixing and was calcined at 1273 K for 6 hours. The calcined powder was then pressed into a pellet in 6 mm in diameter. Sintering was carried out by placing the powder compact into a sealed zirconia tube that was connected to a pressure control valve (Fig.22). Prior to the sintering, oxygen gas at  $\sim 6.25$  atm was filled into the sealed zirconia tube after the evacuation. Upon heating, the pressure of sealed oxygen gas increased and reached  $\sim 13$  atm when the powder compact was sintered at 1573K for 2 hours. This eventually led to formation of dense polycrystalline AgTaO<sub>3</sub>.

1  
23  
4

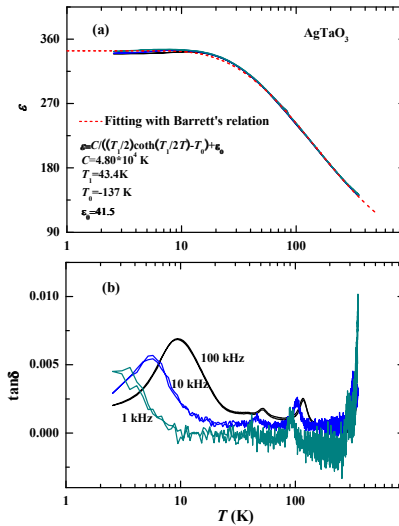
5 Fig. 22. Schematic diagram of the self-customized furnace employed for the sintering at high  
6 oxygen pressure.

## 7 6.2 Phase formation and dielectric behaviors

8 X-ray diffraction analyses (Fig.23) suggest the  $\text{AgTaO}_3$  is rhombohedral with  $R\bar{3}c$   
9 symmetry at room temperature (Wołczyr & Łukaszewski, 1986). Diffraction patterns  
10 obtained at 68.4 K remain unchanged, indicating that such nonpolar phase persists down to  
11 low-temperatures. This is also supported by the measurements on the dielectric constants  
12 (Fig.24) and heat capacity (Fig.25), in which no anomaly was probed in the low  
13 temperatures.

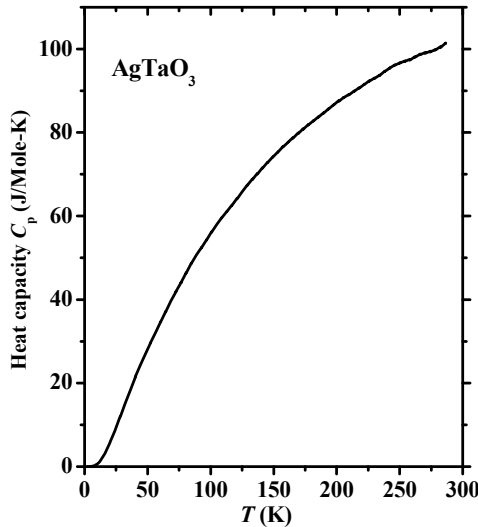
14  
1516  
17

18 Fig. 23. XRD traces for  $\text{AgTaO}_3$  obtained at 300 K and 68.4 K together with the standard  
19 pattern given by the powder diffraction file (PDF) No. 01-072-1383.



1  
2  
3  
4

Fig. 24. Temperature dependence of (a)  $\epsilon$  together with the fitting to the Barrett's relation indicated by the dashed line and (b)  $\tan\delta$  for  $\text{AgTaO}_3$  ceramics samples.



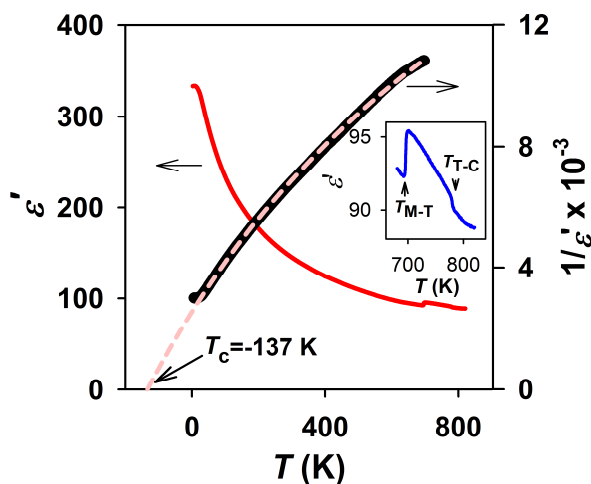
5  
6

Fig. 25. Heat capacity for  $\text{AgTaO}_3$ .

7  
8  
9  
10  
11

Although several frequency-dependent peaks are seen in the dielectric loss (Fig.24(b)), it can be reasonably attributed to polarization relaxations due to defects (Soon et al., 2010). Interestingly, within the low-temperature region, the dielectric behavior follows the Barrett's relation (Barrett, 1952) that is characteristic for the quantum paraelectric system (Abel, 1971; Höchli & Boatner, 1979; Itoh et al., 1999), suggesting that  $\text{AgTaO}_3$  may be a

1 quantum paraelectric. On the other hand, two step-like dielectric anomalies corresponding  
 2 to the phase transitions from monoclinic to tetragonal and tetragonal to cubic were observed  
 3 at 694 and 780 K, respectively, upon heating the samples (Fig.26). This observation is in  
 4 agreement with the previous reports (Kania,1983;Kugel et al., 1987). Furthermore, the  
 5 temperature dependence of  $1/\epsilon$  for  $\text{AgTaO}_3$  shows non-linear behavior, which is similar to  
 6 that of  $\text{KTaO}_3$ , obeying the modified form of the Curie-Weiss law  $\epsilon = \epsilon_L + C/(T - T_0)$  (Rupprecht  
 7 & Bell, 1964).  
 8



9  
 10 Fig. 26. Temperature dependences of  $\epsilon'$  and  $1/\epsilon'$  fitted to the modified Curie-Weiss law  
 11  $\epsilon = \epsilon_L + C/(T - T_0)$  (dashed line,  $\epsilon_L = 38.2$ ,  $C = 4.7 \cdot 10^4$  K,  $T_0 = 137$  K) for  $\text{AgTaO}_3$  measured at 1  
 12 MHz upon heating. The inset further shows the step-like phase transitions from monoclinic  
 13 to tetragonal and then to cubic at  $T_{M-T} = 694$  K and  $T_{T-C} = 780$  K, respectively.

## 14 7. $(\text{Ag}_{1-x}\text{Li}_x)\text{TaO}_3$ solid solution

15 Similar to the case of  $\text{AgNbO}_3$ , ~12 mole% of Li can be incorporated into the Ag-site of  
 16  $\text{AgTaO}_3$  to form  $(\text{Ag}_{1-x}\text{Li}_x)\text{TaO}_3$  (Soon et al., 2009). Although the transition temperature is  
 17 lower than room temperature, ferroelectricity can be induced in this solid solution due to  
 18 the strong off-centering nature of the small Li ions.

### 19 7.1 Synthesis

20  $(\text{Ag}_{1-x}\text{Li}_x)\text{TaO}_3$  was prepared by the conventional solid-state reaction with  $\text{Ag}_2\text{O}$ ,  $\text{Ta}_2\text{O}_5$  and  
 21  $\text{Li}_2\text{CO}_3$ , where the powder mixture was calcined at 1273 K for 6 hours. The calcined powder  
 22 was then pressed into a pellet with 6 mm in diameter. Sintering was carried out by the same  
 23 high-pressure process used for pure  $\text{AgTaO}_3$ , which eventually led to formation of dense  
 24 ceramics samples of  $(\text{Ag}_{1-x}\text{Li}_x)\text{TaO}_3$

### 25 7.2 Dielectric behaviours and confirmation of ferroelectric phase

26 Figures 27 & 28 plot the temperature dependence of dielectric constant  $\epsilon$  and loss  $\tan\delta$  for  
 27  $(\text{Ag}_{1-x}\text{Li}_x)\text{TaO}_3$  with  $x \leq 0.12$  obtained at frequencies ranging from 1 kHz to 1 MHz,

1 respectively. It can be seen that a dielectric peak was gradually induced by  $\text{Li}^+$  substitution  
2 in  $\text{AgTaO}_3$ . In contrast to the single peak of the dielectric constant, there are two to four  
3 peaks of the dielectric loss within the same temperature window. Since the additional loss  
4 peaks do not associate with a remarkable change in the dielectric constant, it is very likely  
5 due to the defect effects dependent with sample processing. It can be seen that a well-  
6 defined peaks has occurred in the  $\sim$ MHz frequency regions for the substitution at extremely  
7 low level, for example, at  $x=0.02$ . This indicates the existence of local polarization in the  
8 doped crystal (Vugmeister & Glinchuk, 1990; Samara, 2003). This fact again suggests that  
9  $\text{AgTaO}_3$  is actually under a critical state of the quantum paraelectric. Any slight modification  
10 will lead to the appearance of observable polarization in the system. For small substitution,  
11 the location of the dielectric anomaly depends on the observed frequency. Figure 29 gives an  
12 evaluation on this frequency dependence. In the figure, the temperature-axis is scaled with  
13 the peak position of 1 MHz, making it easy to see the change with composition. For  $x=0.008$ ,  
14 the frequency dispersion is very strong, peak position of the dielectric constant shifts about  
15 50% with respect to that of 1 MHz for  $f=1$  kHz. However, for  $x=0.035$ , such change is less  
16 than 2%, meaning that ferroelectric phase transition temperature  $T_c$  is well defined in the  
17 sample. Thus, we can infer that a macroscopic ferroelectric phase is evolved below  $T_c$  in this  
18 composition. This was also confirmed by the results shown in Fig.30, in which ferroelectric  
19 loop was obtained for  $T < T_c$  for a sample with  $x=0.12$  that has the same dielectric behaviors  
20 to that of  $x=0.035$ .

21 On the basis of the above results, a phase diagram is proposed in Fig.31, in which PE and FE  
22 represents the paraelectric and ferroelectric phases, respectively. As mentioned above, since  
23 the peak of the dielectric constant is strongly dependent with frequency for  $0 < x < 0.035$ , the  
24 gray zone in the phase diagram may be attributed to dipole-glass phase (Vugmeister &  
25 Glinchuk, 1990; Pirc & Blinc, 1999; Samara, 2003) or a phase with nanosized ferroelectric  
26 domains (Fisch, 2003; Fu et al., 2009b), which remains to be addressed by further  
27 investigations.

## 28 8. Concluding remarks

29 Our recent works reveal that silver perovskites are of great interests from either the view-  
30 point of fundamental research or that of application research in the fields of ferroelectric or  
31 piezoelectric. Promising ferroelectric and piezoelectric properties have been demonstrated  
32 in some compounds such as  $(\text{Ag},\text{Li})\text{NbO}_3$  and  $(\text{Ag},\text{K})\text{NbO}_3$  alloys, but further works are  
33 required to improve the material performance, to understand the basic physics of the  
34 ferroelectricity/piezoelectricity of the materials, and to seek novel promising compound  
35 among the discovered solutions or alloys with other ferroelectric systems. Moreover,  
36 integration techniques of thin films are also a direction for the future work when  
37 considering the practical applications.

## 38 9. Acknowledgment

39 Part of this work was supported by the Collaborative Research Project of Materials and  
40 Structures Laboratory of Tokyo Institute of Technology, and Grant-in-Aid for Scientific  
41 Research, MEXT, Japan.

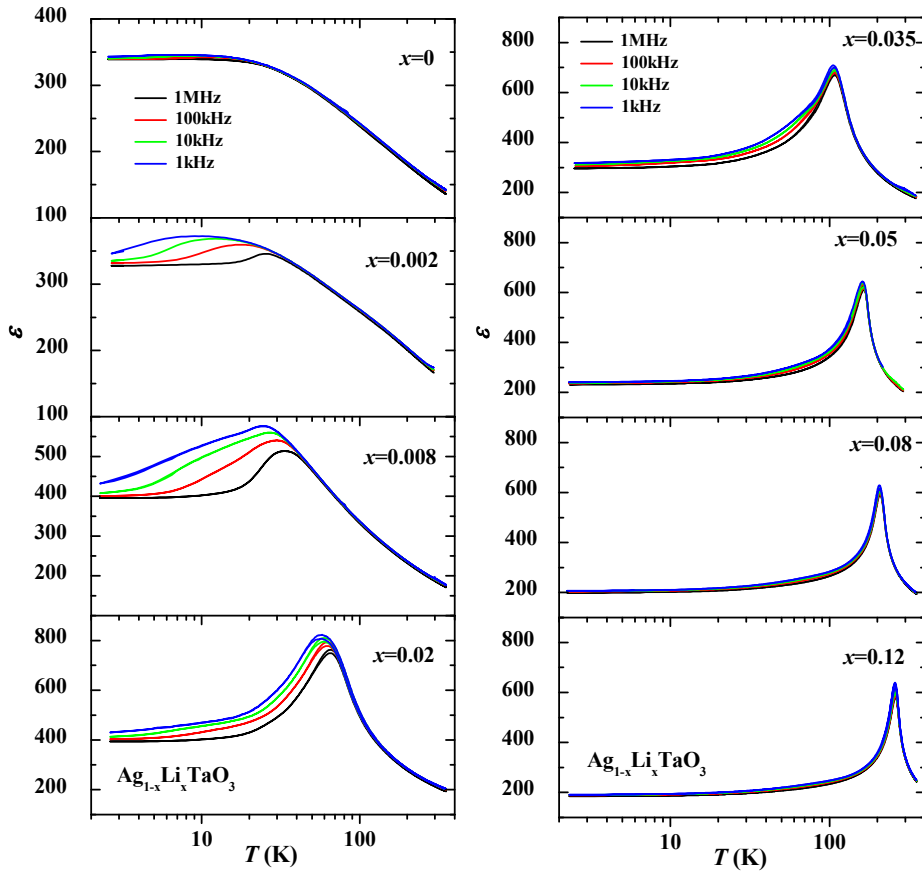
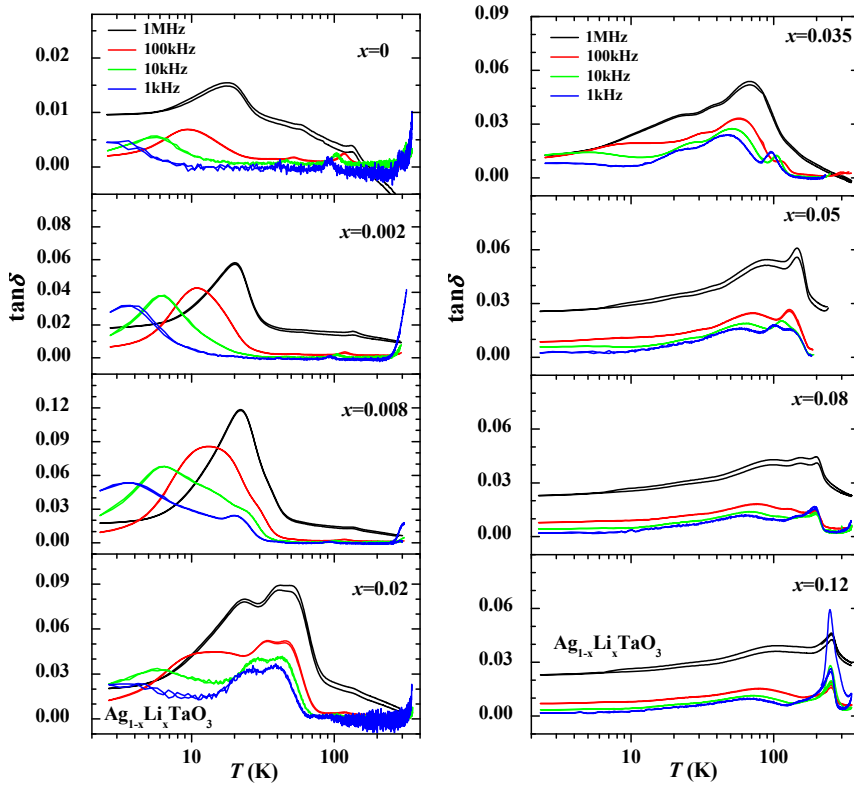
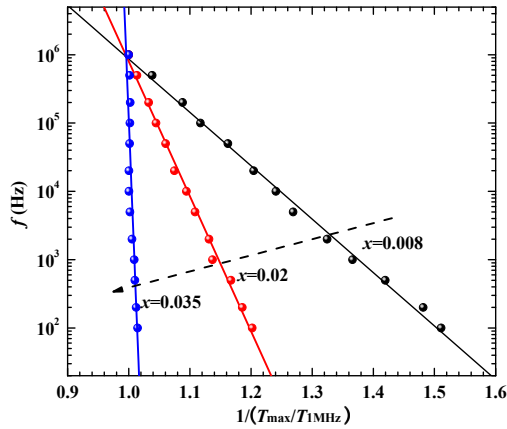
1  
2  
3  
4  
5  
6  
7  
8  
9  
1011  
12  
13  
14  
15  
16  
17  
18

Fig. 27. Dielectric constant  $\epsilon'(T)$  for  $\text{Ag}_{1-x}\text{Li}_x\text{TaO}_3$  with  $0 \leq x \leq 0.12$ .



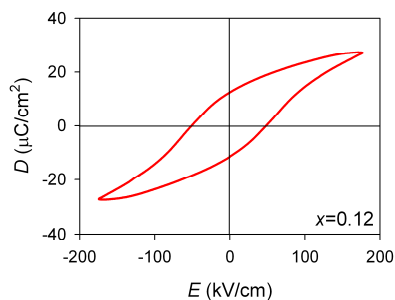
1  
2  
3

Fig. 28. Dielectric loss for  $\text{Ag}_{1-x}\text{Li}_x\text{TaO}_3$  with  $0 \leq x \leq 0.12$ .

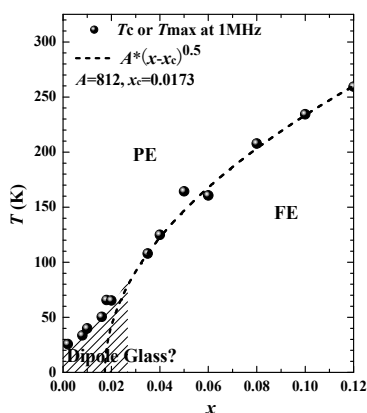


4  
5  
6

Fig. 29. Relationship between frequency and  $T_{\text{max}}$  in  $\text{Ag}_{1-x}\text{Li}_x\text{TaO}_3$ .  $T_{\text{max}}$  was normalized by the  $T_{\text{max}}$  of 1 MHz.



1  
2 Fig. 30. Hysteretic  $D$ - $E$  loop for  $\text{Ag}_{1-x}\text{Li}_x\text{TaO}_3$  with  $x=0.12$  obtained at 0.1 Hz and 77 K,  
3 indicating the ferroelectric state at  $T < T_c$  ( $=258$  K).  
4



5  
6 Fig. 31. Proposed phase diagram for  $\text{Ag}_{1-x}\text{Li}_x\text{TaO}_3$ . The dashed-dotted line shows the fitting  
7 to Morf-Schneider's relationship that is proposed for a quantum phase transition (Morf et  
8 al., 1977). PE and FE denote paraelectric and ferroelectric states, respectively. The gray zone  
9 may be a dipolar-glass state (Pirc & Blinc, 1999) or a state with nanosized ferroelectric  
10 domains (Fisch, 2003; Fu et al., 2009b).

## 11 10. References

- 12 Abel, W. R. (1971). Effect of pressure on the static dielectric constant of  $\text{KTaO}_3$ , *Phys. Rev. B*  
13 4, pp. 2696-2701  
14 Arioka, T. (2009) *Undergraduate thesis of Tokyo Institute of Technology*, Tokyo  
15 Arioka, T.; Taniguchi, H.; Itoh, M.; Oka, K.; Wang, R. & Fu, D. (2010). Ferroelectricity in  
16  $\text{NaNbO}_3$ : Revisited, *Ferroelectrics* 401, pp. 51-55  
17 Baettig, P.; Ederer, C. & Spaldin, N. A. (2005). First principles study of the multiferroics  
18  $\text{BiFeO}_3$ ,  $\text{Bi}_2\text{FeCrO}_6$ , and  $\text{BiCrO}_3$ : Structure, polarization, and magnetic ordering  
19 temperature, *Phys. Rev. B* 72, pp. 214105  
20 Barrett, J. H. (1952). Dielectric Constant in perovskite type crystals, *Phys. Rev.* 86, pp. 118-120

- 1 Bilc, D. I. & Singh, D. J. (2006). Frustration of tilts and A-site driven ferroelectricity in  
2  $\text{KNbO}_3\text{-LiNbO}_3$  alloys, *Phys. Rev. Lett.* 96, pp. 147602
- 3 Cohen, R. E. (1992). Origin of ferroelectricity in perovskite oxides, *Nature* 358, pp. 136-138
- 4 Eglitis, R. I.; Postnikov, A. V. & Borstel, G. (1997). Semiempirical Hartree-Fock calculations  
5 for pure and Li-doped  $\text{KTaO}_3$ , *Phys. Rev. B* 55, pp. 12976-12981
- 6 Egami, T.; Dmowski, W.; Akbas M. & Davies, P. K. (1998). Local structure and polarization  
7 in Pb containing ferroelectric oxides in *First-Principles Calculations for Ferroelectrics –*  
8 *5th Williamsburg Workshop* ed Cohen R., pp 1-10, AIP, New York
- 9 Fabry, J.; Zikmund, Z.; Kania, A. & Petricek, V. (2000). Silver niobium trioxide,  $\text{AgNbO}_3$ ,  
10 *Acta Cryst.* C56, pp. 916-918
- 11 Fisch, R. (2003). Random-field models for relaxor ferroelectric behavior, *Phys. Rev. B* 67, pp.  
12 094110
- 13 Fu, D.; Endo, M.; Taniguchi, H.; Taniyama, T. & Itoh, M. (2007).  $\text{AgNbO}_3$ : A lead-free  
14 material with large polarization and electromechanical response, *Appl. Phys. Lett.*  
15 90, pp. 252907
- 16 Fu, D.; Endo, M.; Taniguchi, H.; Taniyama, T.; Koshihara, S. & Itoh, M. (2008) Piezoelectric  
17 properties of lithium modified silver niobate perovskite single crystals, *Appl. Phys.*  
18 *Lett.* 92, pp. 172905
- 19 Fu, D.; Itoh, M. & Koshihara, S. (2009a). Dielectric, ferroelectric, and piezoelectric behaviors  
20 of  $\text{AgNbO}_3\text{-KNbO}_3$  solid solution, *J. Appl. Phys.* 106, pp. 104104
- 21 Fu, D.; Taniguchi, H.; Itoh, M.; Koshihara, S.; Yamamoto, N. & Mori, S. (2009b). Relaxor  
22  $\text{Pb}(\text{Mg}_{1/3}\text{Nb}_{2/3})\text{O}_3$ : A ferroelectric with multiple inhomogeneities, *Phys. Rev. Lett.*  
23 103, pp. 207601.
- 24 Fu, D.; Itoh, M. & Koshihara, S. (2010). Invariant lattice strain and polarization in  $\text{BaTiO}_3\text{-}$   
25  $\text{CaTiO}_3$  ferroelectric alloys, *J. Phys.: Condens. Matter* 22, pp. 052204
- 26 Fu, D.; Endo, M.; Taniguchi, H.; Taniyama, T.; Itoh, M. & Koshihara, S. (2011).  
27 Ferroelectricity of Li-doped silver niobate ( $\text{Ag,LiNbO}_3$ ), *J. Phys.: Condens. Matter* 23,  
28 pp. 075901
- 29 Fortin, W. & Kugel, G. E.; Grigas, J. & Kania, A. (1996). Manifestation of Nb dynamics in  
30 Raman, microwave, and infrared spectra of the  $\text{AgTaO}_3\text{-AgNbO}_3$  mixed system, *J.*  
31 *Appl. Phys.* 79, pp. 4273-4282
- 32 Francombe, M. H. & Lewis, B. (1958). Structural and electrical properties of silver niobate  
33 and silver tantalate, *Acta Cryst.* 11, pp. 175-178
- 34 Goldschmidt, V.M. (1926). *Shrifter Norske Videnskaps-Akad. Oslo, I: Mat.-Naturv. Kl.* No. 2, pp.  
35 8
- 36 Grinberg, I. & Rappe, A. M. (2003). Ab initio study of silver niobate in *Fundamental Physics of*  
37 *Ferroelectrics*, edited by Davies, P. K. & Singh, D. J., pp 130-138, American Institute  
38 of Physics, New York
- 39 Grinberg, I. & Rappe, A. M. (2004). Silver solid solution piezoelectrics, *Appl. Phys. Lett.* 85,  
40 pp. 1760-1762
- 41 Hafid, M.; Kugel, G. E.; Kania, A.; Roleder, K. & Fontana, M. D. (1992). Study of the phase-  
42 transition sequence of mixed silver tantalate niobate ( $\text{AgTa}_{1-x}\text{Nb}_x\text{O}_3$ ) by inelastic  
43 light-scattering, *J. Phys. Condens. Matter.* 4, pp. 2333-2345
- 44 Höchli, U. T. & Boatner, L. A. (1979). Quantum ferroelectricity in  $\text{K}_{1-x}\text{Na}_x\text{TaO}_3$  and  $\text{KTa}_{1-}$   
45  $y\text{Nb}_y\text{O}_3$ , *Phys. Rev B.* 20, pp. 266-275

- 1 Itoh, M.; Wang, R.; Inaguma, Y.; Yamaguchi, T.; Shan, Y.-J. & Nakamura, T. (1999).  
2 Ferroelectricity induced by oxygen isotope exchange in strontium titanate  
3 perovskite, *Phys. Rev. Lett.* 82, pp. 3540-3543
- 4 Jaffe, B.; Cook, Jr., W. R. & Jaffe, H. (1971). *Piezoelectric Ceramics*, Academic, London
- 5 Kania, A. (1983).  $\text{AgNb}_{1-x}\text{Ta}_x\text{O}_3$  solid solutions-dielectric properties and phase transitions,  
6 *Phase Transit.* 3, pp. 131-139
- 7 Kania, A.; Roleder, K. & Lukaszewski, M. (1984). The ferroelectric phase in  $\text{AgNbO}_3$ ,  
8 *Ferroelectrics* 52, pp. 265-269
- 9 Kania, A.; Roleder, K.; Kugel, G. E. & Fontana, M. D. (1986). Raman scattering, central peak  
10 and phase transitions in  $\text{AgNbO}_3$ , *J. Phys. C: Solid State Phys.* 19, pp. 9-20
- 11 Kania, A. (1989). Flux growth of  $\text{AgTa}_x\text{Nb}_{1-x}\text{O}_3$  (ATN) solid solution single crystals, *J. Cryst.*  
12 *Growth* 96, pp. 703-704
- 13 Kania, A. (1998). An additional phase transition in silver niobate  $\text{AgNbO}_3$ , *Ferroelectrics* 205,  
14 pp. 19-28
- 15 Kania, A. & Kwapulinski, J. (1999).  $\text{Ag}_{1-x}\text{Na}_x\text{NbO}_3$  (ANN) solid solutions: from disordered  
16 antiferroelectric  $\text{AgNbO}_3$  to normal antiferroelectric  $\text{NaNbO}_3$ , *J. Phys.: Condens.*  
17 *Matter.* 11, pp. 8933-8946
- 18 Kania, A. (2001). Dielectric properties of  $\text{Ag}_{1-x}\text{A}_x\text{NbO}_3$  (A: K, Na and Li) and  $\text{AgNb}_{1-x}\text{Ta}_x\text{O}_3$   
19 solid solutions in the vicinity of diffuse phase transitions, *J. Phys. D Appl. Phys.* 34,  
20 pp. 1447-1455
- 21 Kato, H.; Kobayashi, H. & Kudo, A. (2002). Role of  $\text{Ag}^+$  in the band structures and  
22 photocatalytic properties of  $\text{AgMO}_3$  (M: Ta and Nb) with the perovskite structure,  
23 *J. Phys. Chem. B* 106, pp. 12441-12447
- 24 Kruczek, M.; Talik, E. & Kania, A. (2006). Electronic structure of  $\text{AgNbO}_3$  and  $\text{NaNbO}_3$   
25 studied by X-ray photoelectron spectroscopy, *Solid State Commun.* 137, pp. 469-473
- 26 Kugel, G. E.; Fontana, M. D.; Hafid, M.; Roleder, K.; Kania, A. & Pawelczyk, M. (1987). A  
27 Raman study of silver tantalate ( $\text{AgTaO}_3$ ) and its structural phase transition  
28 sequence, *J. Phys. C: Solid State Phys.* 20, pp. 1217-1230
- 29 Kuroiwa, Y.; Aoyagi, S.; Sawada, A.; Harada, J.; Nishibori, E.; Takata, M. & Sakata, M.  
30 (2001). Evidence for Pb-O Covalency in Tetragonal  $\text{PbTiO}_3$ , *Phys. Rev. Lett.* 87, pp.  
31 217601
- 32 Levin, I.; Krayzman, V.; Woicik, J. C.; Karapetrova, J.; Proffen, T.; Tucker, M. G. & Reaney, I.  
33 M. (2009). Structural changes underlying the diffuse dielectric response in  $\text{AgNbO}_3$ ,  
34 *Phys. Rev. B* 79, pp. 104113
- 35 Lines, M. E. & Glass, A. M. (1977). *Principle and Application of Ferroelectrics and Related*  
36 *Materials*, Oxford, Clarendon
- 37 Łukaszewski, M.; Kania, A. & Ratuszna, A. (1980). Flux growth of single crystals of  $\text{AgNbO}_3$   
38 and  $\text{AgTaO}_3$ , *J. Cryst. Growth* 48, pp. 493-495
- 39 Łukaszewski, L.; Pawelczyk, M.; Handerek, J. & Kania, A. (1983). On the phase transitions in  
40 silver niobate  $\text{AgNbO}_3$ , *Phase Transit.* 3, pp. 247-258
- 41 Łukaszewski, L. (1983). Dielectric properties of  $\text{Ag}_{1-x}\text{K}_x\text{NbO}_3$  solid solutions, *Ferroelectrics* 44,  
42 pp. 319-324
- 43 Mitchell, R. H. (2002). *Perovskites: modern and ancient*, Almaz press, Ontario
- 44 Morf, R.; Schneider, T. & Stoll, E. (1977). Nonuniversal critical behavior and its suppression  
45 by quantum fluctuations, *Phys. Rev. B* 16, pp. 462-469

- 1 Müller, K. A. & Burkard, H. (1979). SrTiO<sub>3</sub>: An intrinsic quantum paraelectric below 4 K,  
2 *Phys. Rev. B* 19, pp. 3593-3602
- 3 Nalbandyan, V. B.; Medvediev, B. S. & Beliaev, I. N. (1980). Study of the silver niobate-  
4 lithium niobate systems, *Izv.Akad. Nauk SSSR, Neorg. Mater.* 16, pp. 1819-1823
- 5 Paweczyk, M. (1987). Phase transitions in AgTa<sub>x</sub>Nb<sub>1-x</sub>O<sub>3</sub> solid solutions, *Phase Transit.* 8, pp.  
6 273-292
- 7 Petzelt, J.; Kamba, S.; Buixaderas, E.; Bovtun, V.; Zikmund, Z.; Kania, A.; Koukal, V.;  
8 Pokorný, J.; Polivka, J.; Pashkov, V.; Komandin, G. & Volkov, A. (1999). Infrared  
9 and microwave dielectric response of the disordered antiferroelectric Ag(Ta,Nb)O<sub>3</sub>  
10 system, *Ferroelectrics* 223, pp. 235-246
- 11 Pirc, R. & Blinc, R. (1999). Spherical random-bond-random-field model of relaxor  
12 ferroelectrics, *Phys. Rev. B* 60, pp. 13470-13478
- 13 Pisarski, M. & Dmytrow, D. (1987). Phase transitions in ceramic AgNbO<sub>3</sub> investigated at  
14 high hydrostatic pressure, *Ferroelectrics* 74, pp. 87-93
- 15 Ratuszna, A.; Pawluk, J. & Kania, A. (2003). Temperature evolution of the crystal structure of  
16 AgNbO<sub>3</sub>, *Phase Transit.* 76, pp. 611-620
- 17 Reisman, A. & Holtzberg, F. (1958). Heterogeneous equilibria in the systems Li<sub>2</sub>O-, Ag<sub>2</sub>O-  
18 Nb<sub>2</sub>O<sub>5</sub> and oxide-models. *J. Am. Chem. Soc.* 80, pp. 6503-6507
- 19 Rodel, J. Jo, W.; Seifert, K. T. P.; Anton, E.; Granzow, T. & Damjanovic, D. (2009). Perspective  
20 on the development of lead-free piezoceramics, *J. Am. Ceram. Soc.* 92, pp. 1153 -1177
- 21 Rupprecht, G. & Bell, R. O. (1964). Dielectric constant in paraelectric perovskites, *Phys. Rev.*  
22 135, pp. A748-A752
- 23 Saito, Y.; Takao, H.; Tani, T.; Nonoyama, T.; Takatori, K.; Homma, T.; Nagaya, T. &  
24 Nakamura, M. (2004). Lead-free piezoceramics, *Nature* 432, pp. 84-87
- 25 Sakabe, Y.; Takeda, T.; Ogiso, Y. & Wada, N. (2001). Ferroelectric Properties of (Ag,  
26 Li)(Nb,Ta)O<sub>3</sub> Ceramics, *Jpn. J. Appl. Phys. Part 1*, 42 pp. 5675-5678
- 27 Samara, G. A. (2003). The relaxational properties of compositionally disordered ABO<sub>3</sub>  
28 perovskite. *J. Phys.: Condens. Matter* 15, pp. R367-R411
- 29 Sano, R., Morikawa, D.; Tsuda, K.; Fu, D. & Itoh, M. (2010). Space group determination of  
30 AgNbO<sub>3</sub> at room temperature by CBED method, *Meeting abstracts of the physical  
31 society of Japan* 65 (issue 2, part 4), pp. 916
- 32 Sciau, Ph; Kania, A.; Dkhil, B.; Suard, E. & Ratuszna, A. (2004). Structural investigation of  
33 AgNbO<sub>3</sub> phases using x-ray and neutron diffraction, *J. Phys.: Condens. Matter* 16,  
34 pp. 2795-2810
- 35 Scott, J. F. (2000). *Ferroelectric Memories*, Springer, Berlin
- 36 Shannon, R. D. (1976). Revised effective ionic radii and systematic studies of interatomic  
37 distances in halides and chalcogenides, *Acta Crystallogr., Sect. A: Cryst. Phys., Diffr.,  
38 Theor. Gen. Crystallogr.* 32, pp. 751-767
- 39 Shigemi, A.; Wada, T. (2008). Crystallographic phase stabilities and electronic structures in  
40 AgNbO<sub>3</sub> by first-principles calculation, *Molecular Simulation* 34, pp. 1105-1114
- 41 Shiozaki, Y.; Nakamura, E. & Mitsui, T. (2001). *Ferroelectrics and Related Substances*, Vol. 36,  
42 Pt. A1, Springer, Berlin
- 43 Soon, H. P.; Taniguchi, H. & Itoh, M. (2010). Dielectric and soft-mode behaviors of AgTaO<sub>3</sub>,  
44 *Phys. Rev. B* 81, pp. 104105
- 45 Soon, H. P.; Taniguchi, H. & Itoh, M. (2009). Ferroelectricity triggered in the quantum  
46 paraelectric AgTaO<sub>3</sub> by Li-substitution, *Appl. Phys. Lett.* 95, pp. 242904

- 1 Takeda, T.; Takahashi, Y.; Wada, N. & Sakabe, Y. (2003). Effects of substitution of Na and K  
2 ions for Ag ion in (Ag,Li)NbO<sub>3</sub> Ceramics, *Jpn. J. Appl. Phys. Part 1*, 42, pp. 6023-  
3 6026
- 4 Uchino, K. (1997). *Piezoelectric Actuators and Ultrasonic Motors*, Kluwer Academic, Boston
- 5 Valant, M.; Axelsson, A.; Alford, N. (2007a). Review of Ag(Nb,Ta)O<sub>3</sub> as a functional  
6 material, *J. Euro. Ceram. Soc.* 27, pp. 2549-2560
- 7 Valant, M.; Axelsson, A.; Zou, B. & Alford, N. (2007b). Oxygen transport during formation  
8 and decomposition of AgNbO<sub>3</sub> and AgTaO<sub>3</sub>, *J. Mater. Res.* 22, pp. 1650-1655
- 9 Verwerft, M.; Dyck, D. V.; Brabers, V. A. M.; Landuyt, J. V. & Amelinckx S. (1989). Electron  
10 microscopic study of the phase transformations in AgNbO<sub>3</sub>, *Phys. Stat. Sol. (a)* 112,  
11 pp. 451-466
- 12 Volkov, A. A.; Gorshunov, B. P.; Komandin, G.; Fortin, W.; Kugel, G. E.; Kania, A. & Grigas,  
13 J. (1995). High-frequency dielectric spectra of AgTaO<sub>3</sub>-AgNbO<sub>3</sub> mixed ceramics, *J.*  
14 *Phys.: Condens. Matter* 7, pp. 785-793
- 15 Vugmeister, B. E. & Glinchuk, M. D. (1990). Dipole glass and ferroelectricity in random-site  
16 electric dipole systems, *Rev. Mod. Phys.* 62, pp. 993-1026
- 17 Wada, S., Park, S.-E.; Cross, L. E. & Shrout, T. R. (1998). Domain configuration and  
18 ferroelectric related properties of relaxor based single crystals, *J. Korean Phys. Soc.*  
19 32, pp. S1290-S1293
- 20 Weirauch, D. F. & Tennery, V. (1967). Electrical, X-Ray, and thermal expansion studies in the  
21 system KNbO<sub>3</sub>-AgNbO<sub>3</sub>, *J. Am. Ceram. Soc.* 50, pp. 671-673
- 22 Wołczyr, M. & Łukaszewski, M. (1986). The crystal structure of the room-temperature phase  
23 of AgTaO<sub>3</sub>. *Zeitschrift für Kristallographie* 177, pp. 53-58
- 24 Yashima, M.; Matsuyama, S.; Sano, R.; Itoh, M.; Tsuda, K. & Fu, D. (2011). Structure of  
25 ferroelectric silver niobate AgNbO<sub>3</sub>, *Chem. Mater.* 23, pp. 1643-1645  
26